Hindawi
Adsorption Science & Technology
Volume 2022, Article ID 3786561, 14 pages
https://doi.org/10.1155/2022/3786561

Research Article

α and γ Alumina Spheres for Azo Dye (Allura Red) Removal from Aqueous Media

Jonatan Torres-Pérez,[1] **Nahum Medellín-Castillo**,[2] **and Simón Yobanny Reyes-López**[3]

[1]*Laboratorio de Transferencia y Degradación de Contaminantes, Instituto de Ciencias Biomédicas, Departamento de Ciencias Químico Biológicas, Universidad Autónoma de Ciudad Juárez, Anillo Envolvente del Pronaf y Estocolmo s/n, Zona Pronaf, Ciudad Juárez, Chihuahua C.P. 32310, Mexico*
[2]*Centro de Investigación y Estudios de Posgrado, Facultad de Ingeniería, Universidad Autónoma de San Luis Potosí, Av. Dr. Manuel Nava No. 8, San Luis Potosí SLP 78210, Mexico*
[3]*Laboratorio de Materiales Híbridos Nanoestructurados, Instituto de Ciencias Biomédicas, Departamento de Ciencias Químico Biológicas, Universidad Autónoma de Ciudad Juárez, Anillo Envolvente del Pronaf y Estocolmo s/n, Zona Pronaf, Ciudad Juárez, Chihuahua C.P. 32310, Mexico*

Correspondence should be addressed to Jonatan Torres-Pérez; jonatan.torres@uacj.mx

Received 16 March 2022; Revised 8 April 2022; Accepted 13 April 2022; Published 4 May 2022

Academic Editor: Anjani Ravi Kiran Gollakota

Allura red or Red 40 (R40) is a dye widely used in the food, textile, and pharmaceutical industries; it is considered dangerous because it is soluble in water, and it has high toxicity and resistance to natural degradation. Several advanced wastewater treatments have been shown to be effective for R40 removal but some of them present disadvantages such as by-products obtention, high energy consumption, and high cost of the reactants used in the removal process. In the present work, α-Alumina (Alu) and γ-Alu spheres were synthesized by the encapsulation method. The prepared spheres were characterized by FT-IR, XRD, SEM/EDS, and S_{BET}, and it was determined the presence of only inorganic bonds from ceramic material, and the amorphous alumina was observed in spheres with a smooth and uniform surface and with pores. R40 adsorption kinetics and isotherms were performed, as well as material regeneration for consequent sorption cycles. Sorption tests for R40 removal were carried out under different conditions of initial concentration, pH value, and the presence of interfering ions. The maximal sorption capacity of the synthetized α- and γ-Alu spheres were situated between 0.1765 and 18.9865 mg/g. Different kinetic and isothermal equations were applied and finally, the experimental data was described by Elovich and Freundlich models. The γ-Alu spheres after five heat treatment regeneration cycles showed stable behavior and potential re-use in new sorption processes with R40 removal >97.7% at pH 3 and >85.6% at C_0 =10 mg/L. The obtained results showed that the γ-Alu spheres are novel, alternative, and sustainable synthesized materials for the advanced treatment of wastewater by adsorption process for the removal of Allura red azo dye in aqueous media.

1. Introduction

Azo dyes are the largest group of synthetic organic dyes, and most of the colored molecules are used in the textile and food industry. Large amounts of dyes are disposed into the sewer system, so the elimination from wastewater presents a greater challenge than the treatment of other organic and inorganic compounds that are degraded by conventional treatments. Azo dyes are the most used synthetic organic compounds to give color to a great variety of commercial products and these kinds of dyes have the particularity to contain one or more azo groups (N=N). One of the most popular azo dyes used around the world is Allura Red (R40) and it has been proved in previous studies that it is carcinogenic and mutagenic [1]. Therefore, there is an urgency to develop effective methods for the advanced

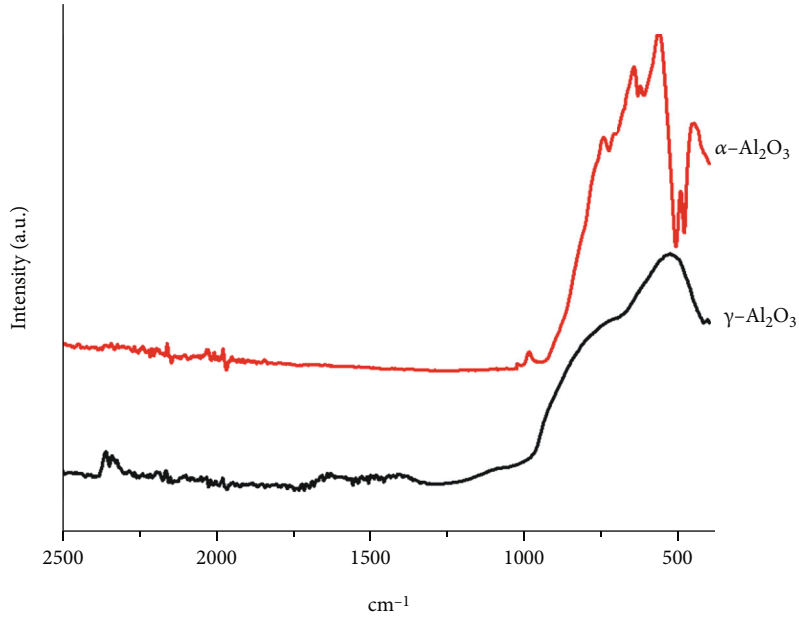

Figure 1: Infrared spectra for α-Alu and γ-Alu spheres.

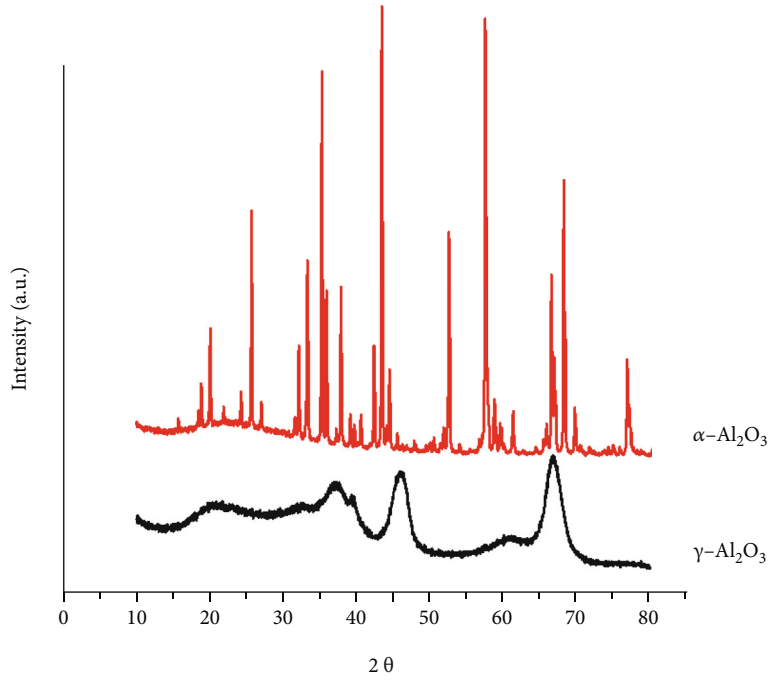

Figure 2: Diffraction patterns for α-Alu and γ-Alu spheres.

treatment of wastewater contaminated with organic azo dyes. Several treatment methods have been developed; however, most of the applied technologies are ineffective since they generate by-products that are sometimes molecules with greater toxicity than the original compound [2, 3].

An advanced water treatment technique is adsorption, which has been proved to be one of the most effective and economical treatments; its application is easy as well as its operation and profitability, in addition to the fact that, unlike other technologies, it does not generate secondary by-products, which transforms this technology into a highly sustainable alternative for polluted water treatment. The materials that have been used throughout history in sorption processes have natural or synthetic origin. One of the most used materials for the elimination of dyes from wastewater is activated carbon; however, due to its high cost and manufacturing complexity, several investigations have focused on alternative adsorbents that have a high

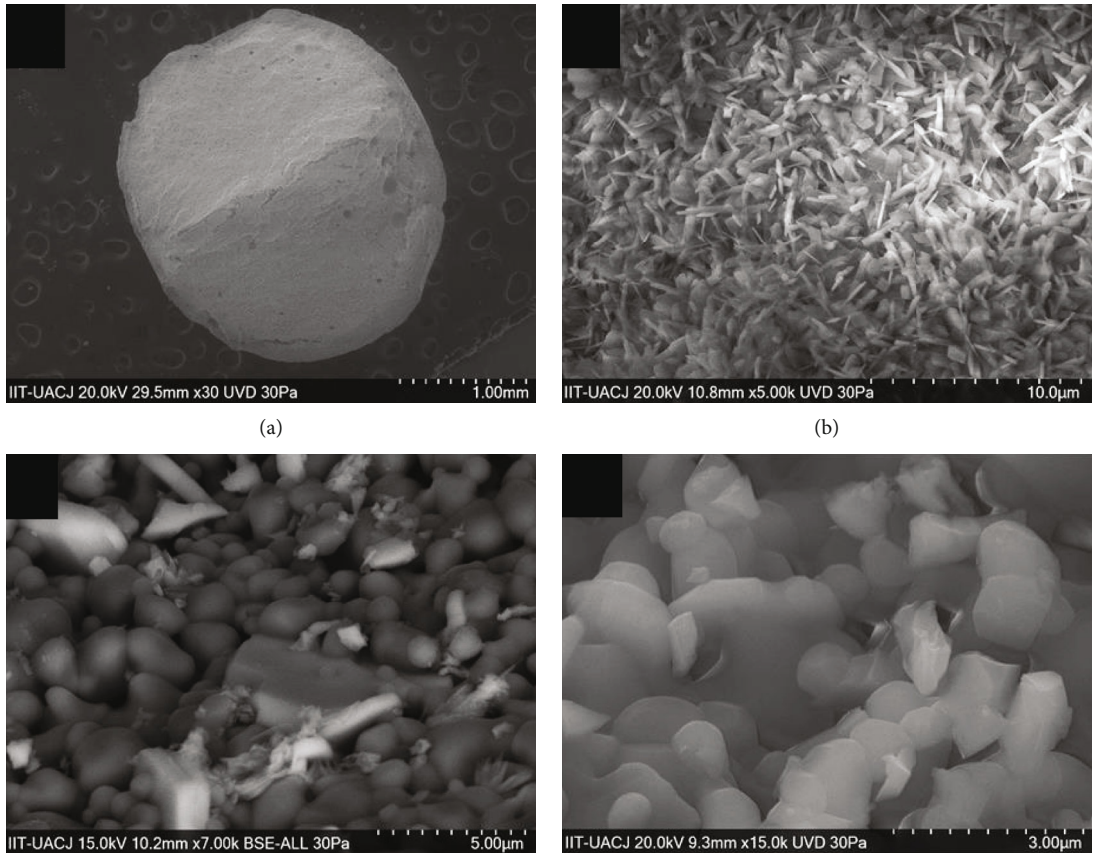

Figure 3: SEM images for α-Alu at (a) 30x, (b) 5000x, (c) 7000x, and (d) 15000x.

adsorption capacity, paying increased attention to synthetic materials [4]. Among the diversity of existing synthetic materials, there are the polymeric and ceramic spheres prepared by encapsulation techniques. Also, alumina spheres have been tested for adsorption of various contaminants from an aqueous solution and their high efficiency has been proven, because they have excellent physical and textural properties. The most abundant metal on Earth is aluminum, which is found in combination with other elements such as oxygen and silicon. Alumina is an oxide composed of this metallic element, and it can be found in bauxite deposits such as gibbsite and boehmite. It is a material that has very good physicochemical properties; however, these depend on the way in which it is synthesized [5]. Other researchers found that the most important polymorphs of alumina are γ-AlOOH, η-Al_2O_3, and α-Al_2O_3, and commonly γ-Al_2O_3 and α-Al_2O_3 are used as adsorbents, catalysts, and catalytic supports [6, 7].

The use of gamma-alumina (γ-Alu) as an adsorbent and catalyst support stands out because it has a large surface area, high stability, and several acid/base sites. Previous research has been elaborated γ-Alu nanoparticles for the removal of yellow eosin dye; the kinetic test was carried out at pH 4 where it was obtained a 99.36% dye removal [8]. Several adsorption models were used, and the Langmuir isotherm was the one that best described the sorption process because it obtained a high correlation coefficient.

A previous study prepared porous γ-Alu microspheres using the modified spray drying method [9]; the material was employed to eliminate the Congo Red dye and it had great retention capacity. In another study, Congo Red has been removed from an aqueous medium with manufactured porous microspheres of ZnO-Al_2O_3; the material had good adsorption performance compared to ZnO and pure Al_2O_3, since the composite has more specific surface area [10]. However, there are no reports of studies about the removal of R40 azo dye onto α- and γ-Alumina spheres converting these materials into novel alternatives for the advanced treatment of water contaminated with organic pollutants.

2. Materials and Methods

2.1. Preparation of Sodium Alginate, Polyvinyl Alcohol (PVA), and Barium Chloride Solutions. A 10% sodium alginate solution was prepared by dissolving 1 g of sodium alginate in 10 mL of deionized water. The mixture was heated to 60°C with constant stirring until the alginate was completely dissolved. The PVA solution was prepared at 7%, and 1.75 g of PVA was dissolved in 25 mL of deionized water. The mixture was heated to 60°C with constant stirring until completely dissolved. The barium chloride solution was prepared at 0.6 M using deionized water.

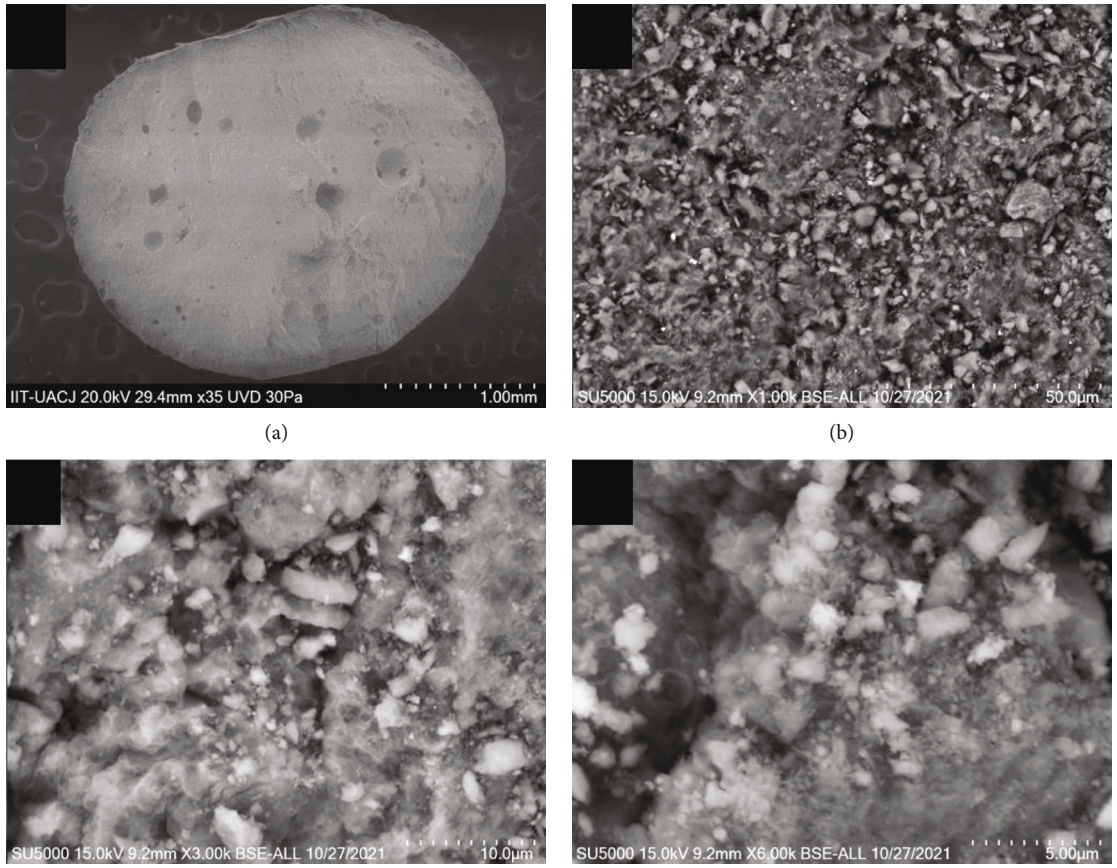

Figure 4: SEM images for γ -Alu at (a) 35x, (b) 500x, (c) 1000x, and (d) 5000x.

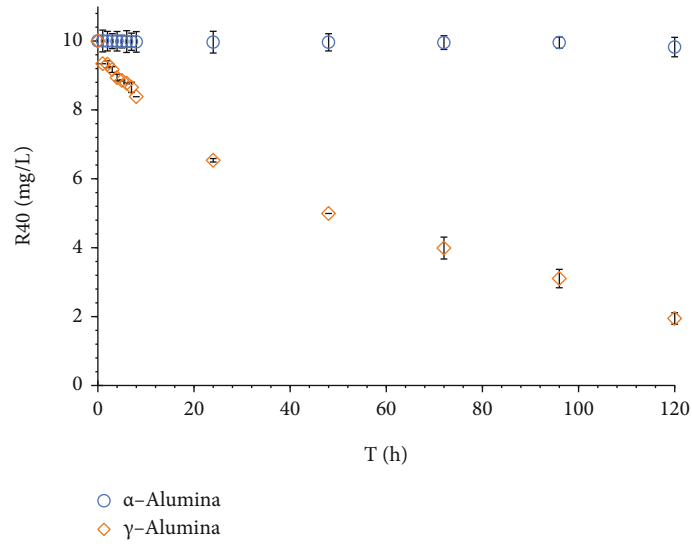

Figure 5: Sorption kinetic test for R40 removal by α-Alu and γ-Alu spheres.

2.2. Suspension of Alumina. A mixture of 1 g of alumina powder, 0.31 g of the 10% sodium alginate solution, 0.15 g of PVA solution, and 0.91 mL of deionized water was made, and finally, the mixture was stirred at 25°C and it obtained a white paste. The alumina suspension was dropped into the barium chloride solution. Since the spheres were formed, they were subjected to different heat treatments; the first at 100°C for 24 h (ThermoScientific® oven), the second one at 800°C in a muffle (ThermoScientific®) for 2 h, and the last one was exposed to the highest temperature at 1000°C for

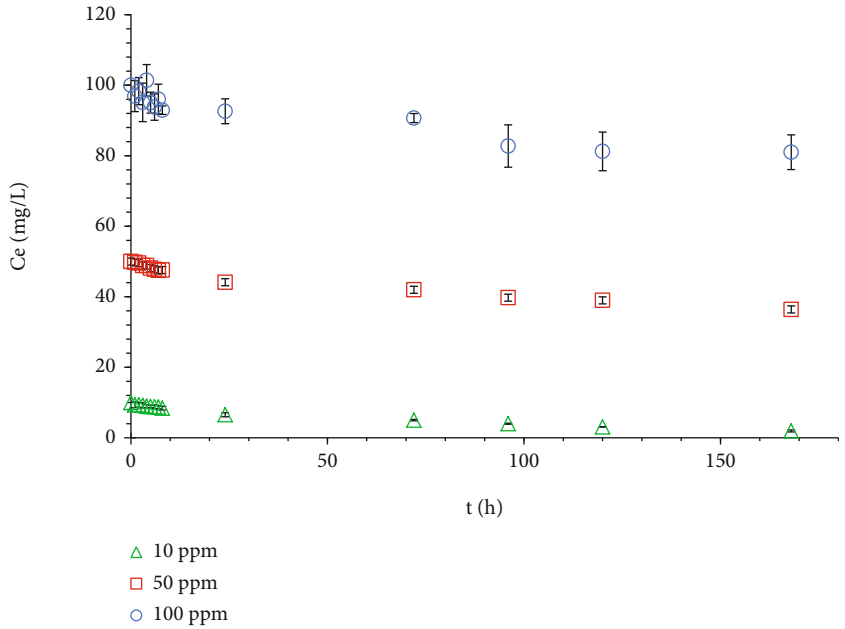

Figure 6: Effect of initial concentration on the sorption of R40 onto γ-Alu spheres.

4 h for γ-Alu and 1600°C for 2 h α-Alu spheres (Nabertherm® oven) [7].

2.3. Characterization of Alumina Spheres. The alumina spheres were characterized by Fourier-transform infrared (FT-IR) spectroscopy, X-ray diffraction (XRD), scanning electron microscope (SEM) with energy-dispersive X-ray spectroscopy (EDS), and specific surface area (SBET).

2.3.1. FT-IR. The FT-IR analysis was employed to determine the chemical groups on the sphere's surface. The alumina spheres were grounded prior to analysis. A Bruker FT-IR instrument was employed with Platinum-ATR; the analysis was conducted by 32 times scanning (4 cm^{-1}) and measures were done in the 400 and 4000 cm^{-1} intervals [11].

2.3.2. XRD. XRD was used to make an identification of the crystalline phases in alumina spheres. For this analysis, a X'Pert PRO PANalytical instrument (Cu kα=1.54056, 20 kV, 10-80°) was used, and scanning speed of 2°/min.

2.3.3. SEM/EDS. The samples were sputtered with gold employing a Denton Vacuum DeskV instrument. After this procedure, the samples were chemically and morphologically characterized using a Field Emission Scanning Electron microscope SU5000 Hitachi, and JEOL JSM-6010 PLUS/LA Analytical SEM.

2.3.4. S_{BET}. The specific surface area, pore volume, and pore diameter of spheres were measured using N2 and the BET equation, using a physisorption equipment (ASAP2010, Micromeritics). Before analysis, the samples were preheated at 150°C for 2 h to eliminate adsorbed water.

2.4. Sorption Tests. The maximal sorption capacity and the equilibrium time of the alumina spheres were determined by adsorption tests performed with the variation of concentration and pH of the solution. Prior to the sorption tests, the materials were dried for 12 h at 105°C. The specific surface area and pore volume of alumina fibers were measured using N2 and the BET equation, using a physisorption equipment (ASAP2010, Micromeritics). Before analysis, the samples were preheated at 150°C for 2 h to eliminate adsorbed water.

2.5. Sorption Kinetics. For the sorption kinetics, 500 mL was prepared with R40 at 10 ppm for the α-Alu and γ-Alu spheres. This solution was placed in two plastic reactors and then 0.25 g of α-Alu and γ-Alu spheres was added to them. Subsequently, the solutions with the spheres were placed on a Barnstead/Lab-line® A-class plate shaker and were measured every hour for 8 hours and then every 24 hours for 5 days. The concentration of each obtained aliquot was measured at 505 nm wavelength in a Jenway® spectrophotometer (model 7315).

2.5.1. Effect of Initial Concentration. For the initial concentration, three 500 mL solutions were prepared at 10, 50, and 100 ppm. They were divided into six reactors and the concentration was measured at a wavelength of 505 nm; 0.25 g of α-Alu and γ-Alu spheres was weighed and deposited in each of the used reactors. Finally, the solutions with the spheres were shaked and the solutions were sampled every hour for 8 hours and then every 24 hours for 5 days.

2.5.2. Effect of pH. Two batches of 500 mL solution were made with R40 at 10 ppm concentration; subsequently, the pH of the solutions was modified with HCl (0.1 N) or NaOH (0.1 N) to reach pH 3 and 10, respectively, and the value was measured with a Hanna Instruments® potentiometer (Model HI8915). The solutions were placed in two plastic reactors

Table 1: Kinetic parameters from the PFO, PSO, ID, and ELOV models applied to the adsorption process of R40 on the γ-Alu spheres at C_0 =10, 50, and 100 mg/L.

	C_0 =10 mg/L	
Kinetic model	*R40 removal* =81.9793 ± 0.4782%	
	Parameters	
PFO	q_e (mg/g)	8.1979
	$k_{L(h^{-1})}$	0.0177
	R	0.9818
PSO	k (g/mgh)	21.2427
	R	0.9699
ID	k_{id} (mg/g/min)	0.6146
	R	0.9966
ELOV	a	0.6268
	b	0.1662
	R	0.9952
	C_0 = 50 mg/L	
Kinetic model	*R40 removal* =27.1959 ± 0.5776%	
	Parameters	
PFO	q_e (mg/g)	13.5980
	$k_{L(h^{-1})}$	0.0166
	R	0.9830
PSO	k (g/mgh)	76.5649
	R	0.9409
ID	k_{id} (mg/g/min)	1.0129
	R	0.9913
ELOV	a	0.9393
	b	0.0943
	R	0.9944
	C_0 =100 mg/L	
Kinetic model	*R40 removal* =18.9865 ± 4.9235%	
	Parameters	
PFO	q_e (mg/g)	18.9865
	$k_{L(h^{-1})}$	0.0223
	R	0.9045
PSO	k (g/mgh)	433.017
	R	0.9357
ID	k_{id} (mg/g/min)	1.5623
	R	0.9483
ELOV	a	2.6635
	b	0.0879
	R	0.9396

and then 0.25 g of spheres of each material was added. Subsequently, the solutions with the spheres were placed on a Barnstead/Lab-line® A-class plate shaker and these solutions were sampled every hour for 8 hours and then every 24 hours for 5 days. The concentration of each aliquot obtained was measured at a wavelength of 505 nm.

2.6. Sorption Isotherms. Sorption isotherms were made from different solutions of R40 at 1, 2, 3, 4, 5, 6, 7, 8, 9, and 10 ppm as initial concentration. 0.05 g of α-Alu and γ-Alu spheres was placed in 50 mL of the solutions and was left under constant agitation on a Fisher Scientific® brand orbital shaker for 5 days. After this time, an aliquot was taken from each solution and the concentration was measured at 505 nm.

2.6.1. Effect of Ionic Strength. The ionic strength effect over R40 sorption process onto γ-Alu spheres was evaluated. The experimentation was conducted in the same way than it was described previously in the effect of initial concentration section. It was employed a commercial bottled water with specific ion concentrations in it (Ca^{2+} (80 mg/L), HCO^{-}_3 (360 mg/L), Mg^{+2} (26 mg/L), Na^{+} (6.5 mg/L), Si^{+2} (15 mg/L), SO^{-2}_4 (14 mg/L), Cl^{-} (10 mg/L), NO^{-2}_3 (3.8 mg/L), and $CaCO_3$ (300 mg/L).

3. Results and Discussion

In the last years, the research about the synthesis of new and alternative adsorbent materials for water treatment has been increased. Such synthetic materials as α-Alu and γ-Alu spheres have remarkable importance because they have the viability to substitute conventional and non-environmentally friendly materials. The preparation and application of such alternative materials require creative and expert approach of researchers on the basic factors affecting the sorption process of different organic molecules. The characterization of the obtained materials was performed to know their general surface properties. Moreover, their environmental applications were done by comparing the synthetized α-Alu and γ-Alu spheres with their effectiveness to remove R40 azo dye from water, the sorption capacity and removal efficiency determined by sorption experiments.

3.1. Characterization of the Materials

3.1.1. Ft-IR. Figure 1 shows the infrared spectra obtained from α-Alu and γ-Alu spheres. It was not observed typical vibrational bands as evidence of functional groups and bonds present in PVP and alginate. This fact was promoted by decomposition of organic molecules after spheres thermal treatment. Only the inorganic bonds from ceramic material were observed. At 968-400 cm^{-1}, it was observed a wide band that represents the stretching vibration of Al-O bonds in different alumina polymorphs. At 830 and 507-530 cm^{-1} appear bands corresponding to γ-Al_2O_3, and at 800 cm^{-1} and 500-750 cm^{-1} were detected bands from aluminum in tetrahedral (AlO_4) and octahedral (AlO_6) coordination, respectively. The octahedral aluminum of α-alumina generates bands placed at 438-456, 491-499, 550, 576-601, 635-644, and 755-763 cm^{-1} [6]. The materials after dye sorption were analyzed; therefore, no changes were observed in the FT-IR spectra because the presence of the R40 on the surface was not in amounts to be detected by the instrument (figure does not show).

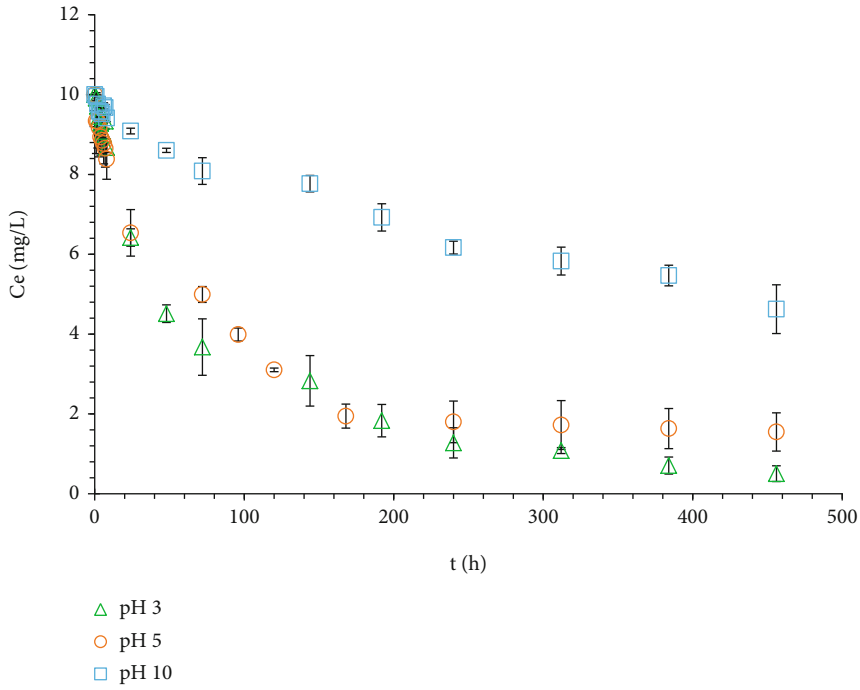

Figure 7: Effect of pH on the sorción of R40 onto γ-Alu spheres.

3.1.2. XRD. Figure 2 shows diffraction patterns of α-Alu and γ-Alu spheres; small non-defined crystallographic peaks in the diffractogram are evidence of the presence of amorphous alumina in spheres. γ-Alu crystalline planes (222), (400), and (400) are located at 39°, 46°, and 67°, respectively; the γ-Alu characteristic peaks disappear at 1600°C to give a phase transition to α-alumina phase. The turnover is represented by the peak's appearance at 25, 35, 37.5, 43, 52, 57, 61.5, 66, and 68°, corresponding to (012), (104), (110), (113), (024), (116), (018), (214), and (300) crystalline planes, respectively, when it was compared with JCPDS 83-2081 pattern.

3.1.3. SEM/EDS. Figures 3 and 4 show the micrographs of the α-Alu and γ-Alu spheres; in these micrographs, it is observed that the surface of the alumina sphere is smooth, uniform, and with pores (Figure 3(a)), and the porosity is greater in the γ-Alu sphere according to SEM micrograph magnifications of the studied area (Figures 4(b)–4(d)). Also, it was observed a higher degree of sintering in the α-Alu sphere where there are well-defined grains in the form of hexagonal plates and some small fibers (Figures 3(b)–3(d)); it is reported in the literature that the formation of structures is obtained in sintered α-Alu composites. The materials after dye sorption were analyzed by SEM; therefore, no changes were observed in the images or elemental composition because the presence of the R40 on the surface was not detected by the instrument (figure does not show). EDS analysis was performed on the periphery and on the core of the γ-Alu and α-Alu spheres; the analysis only shows aluminum and oxygen as the main components and traces of barium due to the encapsulation process of the alumina spheres with barium chloride.

3.1.4. Specific Surface Area (S_{BET}). The result of S_{BET} shows a specific surface area of 190 m^2/g, pore volume of 0.52 cm^3/g, and pore diameter 11 nm for γ-Alu and specific surface area of 0.66 m^2/g, pore volume of 0.0016 cm^3/g, and pore diameter 10.19 nm for α-Alu. These results confirm the fact that sintering process forms a more solid mass of ceramic material with low surface areas.

3.2. Azo Dye (R40) Removal

3.2.1. Sorption Kinetics. The removal of R40 was carried out by adsorption with α-Alu and γ-Alu spheres synthesized by the encapsulation method; the results showed that only γ-Alu spheres were capable to remove the R40 dye from aqueous media (82% R40 removal); on the other hand, α-Alu spheres did not show any important sorption capacity (1.8% R40 removal) (Figure 5). Because of these results, the consequent experiments were performed only by using the material that presented sorption capacity (γ-Alu spheres). By increasing the contact time and the initial concentration of R40, the capacity of the sphere to remove the dye continually increased until equilibrium establishment.

(1) Effect of Initial Concentration on Sorption Process. The effect of the R40 initial concentration onto sorption process was conducted at 10, 50, and 100 mg/L. Figure 6 shows the sorption kinetics of γ-Alu spheres and the R40 dye decrease as function of the time. The γ-Alu spheres reached 82, 27, and 19% OTC removal at C_0 =10, 50, and 100 mg/L, respectively.

The effect of contact time on dye sorption such as orange G (OG) by alumina particles was reported previously at 28°C

Table 2: Kinetic parameters from the adjustment of PFO, PSO, ID, and ELOV models applied to the adsorption process of R40 on the γ-Alu spheres at pH =3.0, 5.0, and 10.0 (C_0 =10 mg/L).

	pH 3.0	
Kinetic model	*R40 removal* =94.9610 ± 0.1978%	
	Parameters	
PFO	q_e (mg/g)	9.4961
	$k_{L(h^{-1})}$	0.0147
	R	0.9921
PSO	k (g/mgh)	20.5581
	R	0.9768
ID	k (mg/g/min)	0.5235
	R	0.9683
ELOV	a	0.6806
	b	0.1740
	R	0.9942
	pH 5.0	
Kinetic model	*R40 removal* =84.5150 ± 0.4782%	
	Parameters	
PFO	q_e (mg/g)	8.4515
	$k_{L(h^{-1})}$	0.0177
	R	0.9818
PSO	k (g/mgh)	21.2427
	R	0.9699
ID	k (mg/g/min)	0.6146
	R	0.9966
ELOV	a	0.6268
	b	0.1662
	R	0.9952
	pH 10.0	
Kinetic model	*R40 removal* =53.7524 ± 0.6108%	
	Parameters	
PFO	q_e (mg/g)	5.3752
	$k_{L(h^{-1})}$	0.0051
	R	0.9862
PSO	k (g/mgh)	1.7872
	R	0.9394
ID	k (mg/g/min)	0.2320
	R	0.9917
ELOV	a	0.0807
	b	0.1719
	R	0.9905

and the results showed that the sorption capacity was higher when the contact time rises to 30 min until the equilibrium was reached [12]. This work assumes that the required time to accomplish OG-alumina nanoparticle interactions into equilibrium state was 30 min under the different dye concentrations. In this case, the interaction is independent from initial dye concentrations. In the present study, only γ-Alu spheres showed sorption capacity, but it does not coincide with that result; the time required to attain steady state was higher (more than 24 h). For R40 sorption evaluation on the γ-Alu spheres, the experimental results from sorption tests were adjusted to the pseudo-first order (PFO), pseudo-second order (PSO), intraparticle diffusion (ID), and Elovich (ELOV) models. The PFO equation permitted to discover the sorption capacity of the adsorbent: 8.1, 13.6, and 19.0 mg/g at C_0 =10, 50, and 100 mg/L, respectively, also the sorption rate constants and the correlation coefficients for γ-Alu spheres. The fitting of the experimental results to the equations is described in Table 1. The PFO kinetic model has acceptable R values for 10 and 50 mg/L, showing that the sorption process takes place on a homogeneous surface considered the available sorption sites [13]. When equilibrium was reached approximately between 24 and 48 h, the sorption capacity remains without important changes. The sorption rate becomes a constant value because no more binding sites are available.

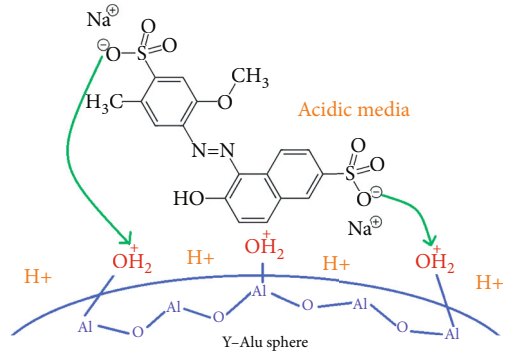

Figure 8: Possible mechanism for R40 sorption onto γ-Alu spheres.

The dye removal at the initial contact time could be due to the sorption sites on the spheres because they were empty and able to retain dye anions from the aqueous phase [14]. As the sorption proceeds on the materials, the rate is getting slow and sorption gets the equilibrium, meaning the active sites saturation. On the other hand, the adjustment to the PSO kinetic model was lower at low concentrations (10 and 50 mg/L), giving the assumption that chemical sorption is the speed limiting step, involving valence forces when sharing or exchanging electrons between spheres and azo dye [15]. When the results were fitted to ELOV, the R value was important (>0.9), then a chemical sorption between the functional groups of the spheres and the dye was done [16].

(2) Effect of pH on Sorption Process. The effect of pH variations (at 3, 5, and 10) of the aqueous solution over the R40 sorption was evaluated through adsorption kinetics (C_0 =10 mg/L). In sorption processes, the pH value is a very important parameter that can affect the sorption capacity of the γ-Alu spheres [17]. The R40 removal improves at low pH values of the media, being 95 and 85% for pH 3 and 5, respectively, and 54% R40 removal for higher pH value (pH =10) (Figure 7). The pH of the system can show

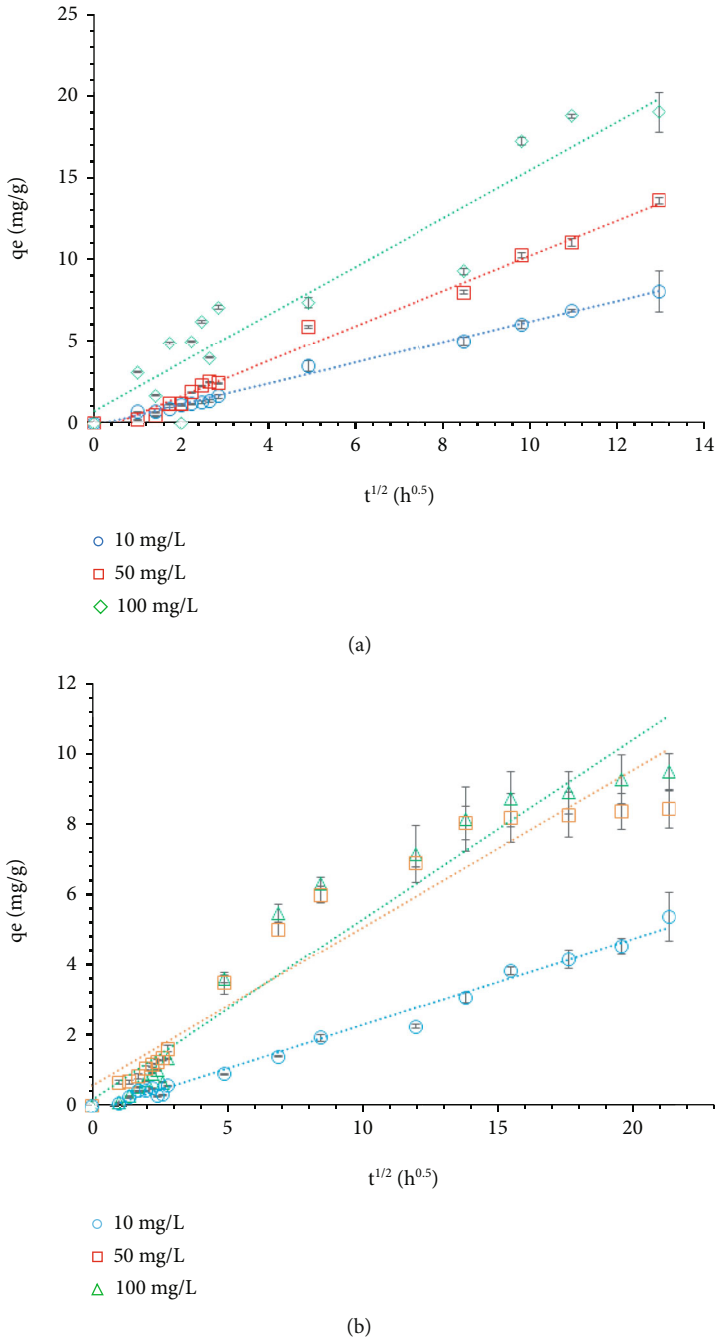

Figure 9: Intraparticle diffusion plots obtained for various sorption processes at (a) different initial concentrations (C_0 =10, 50, and 100 mg/L) and (b) pH values (3, 5, and 10).

higher effect on the uptake of azo dye on γ-Alu spheres' surface. This effect is promoted by the H^+ concentration that establish the total charge of the spheres and the level of ionization/dissociation of the R40 azo dye; this can determine the electrostatic interaction linking the R40 and the γ-Alu spheres. The assessment of the pH effect on the sorption can supply data about the electrostatic interactions [18].

At pH 10, the negative surface charge on the γ-Alu spheres rises, escalating the repulsion by electrostatic interactions between the material and the R40 (54% at pH =10), and because of that, the R40 removal at high pH is lower than at acid pH of the aqueous media. Table 2 shows the kinetic parameters from the fitting of experimental data to PFO, PSO, ID, and Elovich models, and it was observed that the pH modification does not affect the fitting to previous kinetic models. In all cases, the PFO was the equation that describes in better way the sorption process compared to PSO. Moreover, ELOV model fitted to the experimental data, elucidating a chemical sorption of R40 onto the γ-Alu spheres.

The sorption mechanism can be elucidated based on the surface chemistry of the γ-Alu spheres where the presence of

Table 3: Parameters obtained from the adjustment of Langmuir, Freundlich, Temkin, and Dubinin-Radushkevich isotherm models applied to the adsorption process of OTC on the γ-Alu spheres in distilled and ionic water.

Isotherm model	Distilled water *Parameters*	
	b	1.7701
Langmuir	Kt (mg/g)	7.6189
	R	0.9406
	n	0.6360
Freundlich	Kf	4.5980
	R	0.9895
	B	1.4810
Temkin	B_T	1672.9
	R	0.8205
	q_s (mg/g)	7.6189
Dubinin-Radushkevich	KD (mol^2/kJ^2)	-3×10^{-9}
	R	0.9421
Isotherm model	Ionic water *Parameters*	
	b	1.4089
Langmuir	Kt (mg/g)	7.5434
	R	0.9391
	n	0.7202
Freundlich	Kf	3.8771
	R	0.9948
	B	0.4693
Temkin	B_T	5279.2
	R	0.8987
	q_s (mg/g)	7.5434
Dubinin-Radushkevich	KD (mol^2/kJ^2)	-4×10^{-9}
	R	0.9741

a metal oxide in the aqueous phase leads to the hydroxylation of the metal oxide surface [19]. Under these conditions, the metal oxide surface is amphoteric, and it can lead toward acid-base reactions by the pH modification [12].

A possible mechanism of this phenomenon is the pH dependence of the γ-Alu spheres' surface. At high pH values, the net surface charge gets negative due to deprotonation, leading to low sorption of organic molecules because of columbic repulsion. In acidic pH condition (pH = 3 and 5), the surface is positively charged, and is electrostatically attracted to the R40 anionic species leading to a higher adsorption of R40 anions (Figure 8). Other studies have reported the adsorption of anionic dyes with similar behavior [19–21].

The actual mechanistic step that commands the sorption process rate has been reported by other researchers [12] by employing the experimental results from all kinetic tests in the ID model [22]. By plotting a linear relationship and the intercept in zero, it is suitable to determine if the ID model can describe the sorption process and it is indicative of pore diffusion, being in this case the rate controlling step (Figure 9).

The plots of q_e vs $t^{0.5}$ are almost straight over the entire time range, and they are only in one linear section (single segmented plots) in the test at different initial concentrations (Figure 9(a)). In other studies, it was established that the presence of several segments in the plots validates the participation of a phenomenon in multiple stages for the sorption of dyes by alumina nanoparticles [12]. In the case of R40 sorption onto γ-Alu spheres at C_0 = 10, 50, and 100 mg/L (Figure 9(a)), the first linear plot demonstrates external mass transfer, in which the adsorbate migrated through solution to the external surface of the adsorbent resulting in high uptake rate. The results advise that the rate limiting step is intraparticle diffusion and the R40 sorption process is controlled by this mechanism. In the case of pH value variation (pH = 3, 5, and 10), the plot showed only one segment for pH = 10, but at pH = 3 and 5, it was clear that the sorption follows multisegmented plots (Figure 9(b)), indicating that the R40 molecules move into the interior of the γ-Alu spheres by intraparticle diffusion (second linear segment in the plot). Moreover, the rate constant (k_{id}) values (Table 1) have the same trend as that reported for PFO and PSO kinetic models.

3.2.2. Sorption Isotherms. The isotherm tests were applied to obtain data about the interaction between the R40 concentration in water and the amount of R40 removed by the γ-Alu spheres at constant temperature. The experiment was performed by contact test using distilled water and another one with ion strength; the Langmuir, Freundlich, Temkin, and Dubinin-Radushkevich isotherm models were used. The γ-Alu spheres showed q_e = 7.6 mg/g in distilled media and 7.5 mg/g in water with ionic strength.

Equilibrium data obtained by nonlinear fitting of the experimental results provided information of sorption capacity and enabled practical design, and possible use of the materials in advanced water treatment [23]. In a previous study, the sorption capacity of a magnetic nanocomposite (Fe_3O_4@CuS@Ni_2P-CNTs) for R40 removal was tested; the experimental results confirmed the formation of a R40 monolayer onto the adsorbent (Langmuir fitting) at the tested concentration intervals [24]. The Langmuir model is based on the monolayer adsorption of R40 onto homogenous surface of γ-Alu spheres; it assumes that all adsorptive sites are the same and only one molecule is present as thickness. This leads to a surface with specific number of sorption sites, so R40 was retained onto monolayer of synthetized spheres, while Freundlich equation is employed to suppose the multilayer sorption of R40 onto heterogeneous surface [25]. In the present study, the Freundlich model showed the best fitting to the kinetic tests (R > 0.98). The K_f is related to the sorption force and $1/n$ gives an estimation of the R40 sorption intensity [12] being this intensity higher for sorption process in distilled media than ionic water (Table 3). The adsorption capacity of the γ-Alu spheres increased until a maximum of 7.5 mg/g with the R40 concentration increase

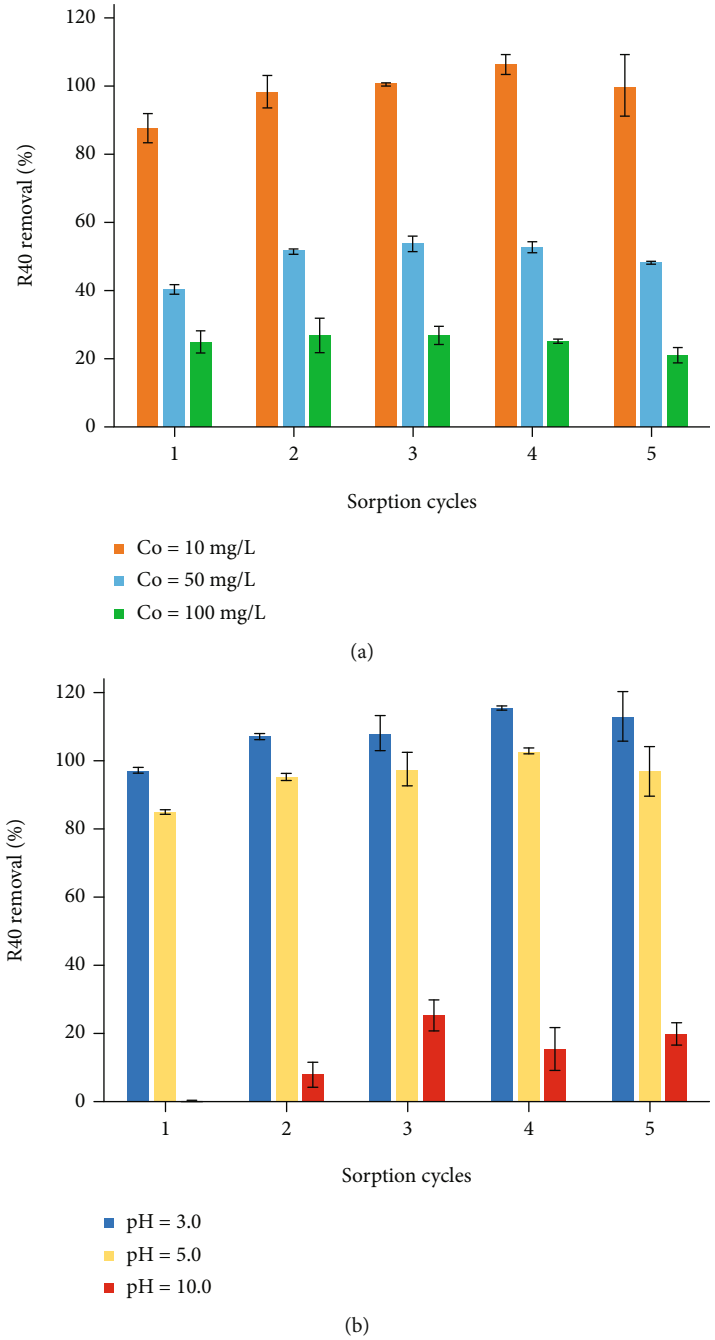

Figure 10: Sorption cycles of R40 onto γ-Alu spheres after regeneration.

in water. The uptake capacity of the adsorbent is a result of high driving force for mass transfer [26].

The application of the Temkin model was useful to obtain the B constant associated to adsorption heat. If B values are placed in the interval of 8 to 16 kJ/mol, the removal of R40 occurs by chemical interactions, but if the value is situated under 8 kJ/mol, the sorption process occurs by physical interactions [27]. This last case occurs for the R40 sorption process of R40 onto γ-Alu spheres in both media (B =0.5 to 1.5 for ions presence and distilled media, respectively). The Dubinin-Radushkevich (D-R) isotherm equations establish a relationship between the size of micropores and the equilibrium sorption ratio; this relation can be indicated by the sorption potential (ε). In a general way, the D-R model is used to describe the sorption mechanisms with a Gaussian energy distribution onto the heterogeneous surface of the adsorbent [28].

In a recent study, the organic dye methylene blue (MB) adsorption onto Al_2O_3 nanofibers was described using the Langmuir and Freundlich isotherm models, and the fitting was better for the Langmuir equation [29]. This indicates that MB adsorption onto porous alumina is carried out by monolayer adsorption process on the adsorbent homogeneous surface, without considering the interaction between

Table 4: Comparison of R40 removal by different adsorbent materials.

Adsorbent material	Sorption capacity q_e (mg/g)	Reference
Zirconia fibers	0.8950	Ávila-Martínez et al. [34]
Activated charcoal (walnut shells)	9.9865	Herrera-García, Aguirre-Ramírez, and Torres-Pérez [35]
Basic anion-exchanger (Lewatit MonoPlus M-600)	3.4120	Wawrzkiewicz and Hubicki [36, 37]
Amberlite IRA-900	9.9950	Wawrzkiewicz and Hubicki [36, 37]
Amberlite IRA-910	10.095	Wawrzkiewicz and Hubicki [36, 37]
Modified organoclay - C3H1	29.400	Ullah et al. [38]
Modified organoclay - C2CB1	25.300	Ullah et al. [38]
Modified organoclay - C2S1	20.300	Ullah et al. [38]
Commercial 4A zeolite (4AZ)	0.4627	Erdoğan [39]
α-Alu spheres (C_0 =10 mg/L)	0.1765	This work
γ-Alu spheres (C_0 =10 mg/L)	8.1979	This work
γ-Alu spheres (C_0 = 50 mg/L)	13.5980	This work
γ-Alu spheres (C_0 =100 mg/L)	18.9865	This work
γ-Alu spheres (pH =3.0)	9.4961	This work
γ-Alu spheres (pH =5.0)	8.4515	This work
γ-Alu spheres (pH =10.0)	5.3752	This work

adsorbate molecules. In the present study, the behavior was opposite (best fitting to Freundlich), inferring that the adsorption process was done onto a heterogeneous surface.

(1) Effect of Competing Ions over R40 Sorption. To study the behavior of the γ-Alu spheres under more realistic conditions, the sorption process was featured under ion strength promoting the contact between adsorbent and adsorbate in aqueous media with presence of calcium, bicarbonates, magnesium, sodium, silicon, sulfates, chlorides, nitrates, and carbonates. The ionic strength in the medium did not significantly affect the performance of the sorption process. The results showed that γ-Alu spheres presented affinity for R40 dye, and the maximum adsorption capacity did not change when it was compared to the sorption tests that take place in distilled media. The interfering ions occupy the sorption sites of the γ-Alu spheres, probably due to a competition between these ions and the R40 molecules. Therefore, in the sorption tests with ionic strength, usually the capacity of the adsorbents to remove molecules is affected [30, 31]. The γ-Alu spheres showed a good fitting to the Langmuir equation (R =0.94) (Table 3), but the fit for Freundlich was better (R =0.99). The n parameter of the Freundlich model was lower than 1, so the spheres showed an important retention of R40 dye. For the Temkin equation, γ-Alu spheres had a better fit with the presence of ions than in distilled media; this suggests that part of the energy of the medium go down while take place interactions between the γ-Alu spheres and the R40 dye [31].

The ionic strength slightly affects the sorption capacity of the γ-Alu spheres. The dependence for R40 sorption decreased when some electrolytes are present in the aqueous media, so a cation exchange could occur as sorption mechanism [32]. In general, other researchers found that ionic strength (SO_4^{2-}) slightly inhibits the organic molecule's elimination by some adsorbents, due to the sorption determined by cation sorption and by H-bonding competition [33].

3.3. Regeneration Cycles. The re-use of the saturated adsorbent materials is a very important topic to ensure the sustainability of the process; this re-use can be achieved by regeneration of the γ-Alu spheres. The regeneration of the adsorbent materials is vital at industrial scales and the option to have access to the use of the adsorbent several cycles without reducing their performance is very important. In the present work, the re-use of γ-Alu spheres was promoted by thermic method (450°C/60 min). After thermal treatment, the sorption process was performed by 5 cycles under the same conditions than the original process (initial concentration of 10, 50, and 100 mg/L and pH values of 3, 5, and 10). The results showed that in almost all the cases, the performance of the γ-Alu spheres was not affected after thermal treatment and in the sorption capacity, it was acceptable along all the 5 sorption cycles for R40 removal (Figure 10).

Other research findings (Table 4) showed that the sorption capacity of different adsorbent materials goes from 0.46 mg/g for a commercial 4A zeolite (4AZ) [39] and higher as 29.4 mg/g for a modified organoclay - C3H1[38]. The q_e values for the synthetized α- and γ-Alu spheres are in the interval of 0.1765 to 18.9865 mg/g; these novel adsorbent materials have interesting sorption capacities compared to those existing already. Moreover, the γ-Alu spheres have important regeneration properties that allow to use them in consequent sorption cycles.

4. Conclusions

The synthesis of adsorbent material by chemical precipitation method was successful for the obtention of α- and γ-

Alu spheres as adsorbent materials. From characterization techniques, it was found that the spheres presented a slight irregular surface and a structure with high mechanical strength. The alumina polymorph is very important because of its hardness and stability. Only the synthesized γ-Alu spheres presented an important percentage of R40 removal at C_0 =10, 50, and 100 mg/L, reaching 81, 14, and 19% removal, respectively, and showed the best fitting to the Elovich equation, advising that the γ-Alu spheres remove R40 azo dye by chemisorption. Acidic pH values were appropriate for the removal of R40.

γ-Alu spheres have a slightly higher sorption capacity for R40 removal in distilled media than in aqueous media with ionic strength. The R40 sorption mechanism can be achieved by cation exchange capacity and electrostatic forces. The results denote the importance to find alternative and sustainable synthesized materials for the advanced treatment of wastewater by adsorption process for the removal of organic dyes (R40) as an emerging pollutant.

Data Availability

The data used to support the findings of this study are available from the corresponding author upon request.

Conflicts of Interest

The authors declare that there are no conflicts of interest.

Authors' Contributions

Jonatan Torres-Pérez contributed to the conceptualization, writing - original draft, and funding acquisition and provided the resources. Nahum Medellín-Castillo contributed to the review and editing. Simón Yobanny Reyes-López contributed to the writing - review and editing.

Acknowledgments

Thanks are due to Judith Véliz for the support in experimental tests and to Universidad Autónoma de Ciudad Juárez (UACJ) for the support to carry out this research and PhD. Mariana Grigoruta from University of Texas at El Paso (UTEP), USA, for English revision.

References

[1] M. Honma, "Evaluation of the *in vivo* genotoxicity of Allura Red AC (Food Red No. 40)," *Food and Chemical Toxicology*, vol. 84, pp. 270–275, 2015.

[2] J. Garcia, H. T. Gomes, J. L. F. Kalck, and J. L. Faria, "Carbon nanotube supported ruthenium catalysts for the treatment of high strength wastewater with aniline using wet air oxidation," *Carbon*, vol. 44, no. 12, pp. 2384–2391, 2006.

[3] F. Gholami-borujeni, M. A. Faramarzi, and F. Nejatzadeh, "Oxidative degradation and detoxification of," *Fresenius Environmental Bulletin*, vol. 22, pp. 739–744, 2013.

[4] V. K. Gupta, "Application of low-cost adsorbents for dye removal - a review," *Journal of Environmental Management*, vol. 90, no. 8, pp. 2313–2342, 2009.

[5] K. Wefers and C. Misra, *Oxides and hydroxides of aluminum*, vol. 19, Alcoa Laboratories, Pittsburgh, 1987.

[6] S. Y. Reyes-López, R. S. Acuña, R. López-Juárez, and J. S. Rodríguez, "Analysis of the phase transformation of aluminum formate Al(O2CH)3 to α-alumina by Raman and infrared spectroscopy," *Journal of Ceramic Processing Research*, vol. 14, no. 5, pp. 627–631, 2013.

[7] J. H. Roque-Ruiz, E. A. Cabrera-Ontiveros, G. González-García, and S. Y. Reyes-López, "Thermal degradation of aluminum formate sol-gel; synthesis of α-alumina and characterization by ^{1}H, ^{13}C and ^{27}Al MAS NMR and XRD spectroscopy," *Results in Physics*, vol. 6, pp. 1096–1102, 2016.

[8] M. S. Thabet and A. M. Ismaiel, "Sol-Gel <i>γ</i>-Al₂O₃ nanoparticles assessment of the removal of eosin yellow using: adsorption, kinetic and thermodynamic parameters," *Journal of Encapsulation and Adsorption Sciences*, vol. 6, no. 3, pp. 70–90, 2016.

[9] M. Li, Z. Si, W. Xiaodong, D. Weng, and F. Kang, "Facile synthesis of hierarchical porous γ-Al_2O_3 hollow microspheres for water treatment," *Journal of Colloid and Interface Science*, vol. 417, pp. 369–378, 2014.

[10] C. Lei, M. Pi, X. Difa, C. Jiang, and B. Cheng, "Fabrication of hierarchical porous ZnO- Al_2O_3 microspheres with enhanced adsorption performance," *Applied Surface Science*, vol. 426, pp. 360–368, 2017.

[11] J. H. Roque-Ruiz, E. A. Cabrera-Ontiveros, J. Torres-Pérez, and S. Y. Reyes-López, "Preparation of PCL/clay and PVA/clay electrospun fibers for cadmium (Cd^{+2}), chromium (Cr^{+3}), copper (Cu^{+2}) and Lead (Pb^{+2}) removal from water," *Water, Air, and Soil Pollution*, vol. 227, no. 8, 2016.

[12] S. Banerjee, S. Dubey, R. K. Gautam, M. C. Chattopadhyaya, and Y. C. Sharma, "Adsorption characteristics of alumina nanoparticles for the removal of hazardous dye, Orange G from aqueous solutions," *Arabian Journal of Chemistry*, vol. 12, no. 8, pp. 5339–5354, 2019.

[13] V. Vadivelan and K. Vasanth Kumar, "Equilibrium, kinetics, mechanism, and process design for the sorption of methylene blue onto rice husk," *Journal of Colloid and Interface Science*, vol. 286, no. 1, pp. 90–100, 2005.

[14] M. Ghaedi, H. Tavallali, M. Sharifi, S. N. Kokhdan, and A. Asghari, "Preparation of low cost activated carbon from Myrtus communis and pomegranate and their efficient application for removal of Congo red from aqueous solution," *Spectrochimica Acta Part A: Molecular and Biomolecular Spectroscopy*, vol. 86, pp. 107–114, 2012.

[15] Y. S. Ho and G. McKay, "The kinetics of sorption of divalent metal ions onto sphagnum moss peat," *Water Research*, vol. 34, no. 3, pp. 735–742, 2000.

[16] H. Qiu, L. Lv, B. C. Pan, Q. J. Zhang, W. M. Zhang, and Q. X. Zhang, "Critical review in adsorption kinetic models," *Journal of Zhejiang University: Science A*, vol. 10, no. 5, pp. 716–724, 2009.

[17] M. Harja and G. Ciobanu, "Studies on adsorption of oxytetracycline from aqueous solutions onto hydroxyapatite," *Science of the Total Environment*, vol. 628-629, pp. 36–43, 2018.

[18] G. M. Ferreira, G. M. Ferreira, M. C. Hespanhol et al., "Adsorption of red azo dyes on multi-walled carbon nanotubes and activated carbon: a thermodynamic study," *Colloids and Surfaces A: Physicochemical and Engineering Aspects*, vol. 529, pp. 531–540, 2017.

[19] M. Wawrzkiewicz, M. Wiśniewska, V. M. Gun'ko, and V. I. Zarko, "Adsorptive Removal of Acid, Reactive and Direct Dyes from Aqueous Solutions and Wastewater Using Mixed Silica–Alumina Oxide," *Powder Technology*, vol. 278, pp. 306–315, 2015.

[20] P. Parthasarathy and S. K. Narayanan, "Effect of hydrothermal carbonization reaction parameters on," *Environmental Progress & Sustainable Energy*, vol. 33, no. 3, pp. 676–680, 2014.

[21] Y. M. Zheng, N. Li, and W. De Zhang, "Preparation of nanostructured microspheres of Zn-Mg-Al layered double hydroxides with high adsorption property," *Colloids and Surfaces A: Physicochemical and Engineering Aspects*, vol. 415, pp. 195–201, 2012.

[22] W. Jr, J. Walter, and J. C. Morris, "Kinetics of adsorption on carbon from solution," *Journal of the Sanitary Engineering Division*, vol. 89, no. 2, pp. 31–59, 1963.

[23] M. Kostić, S. Najdanović, N. Velinov et al., "Ultrasound-assisted synthesis of a new material based on MgCoAl-LDH: Characterization and optimization of sorption for progressive treatment of water," *Environmental Technology and Innovation*, vol. 26, article 102358, 2022.

[24] A. Asfaram, M. Ghaedi, H. Abidi, H. Javadian, M. Zoladl, and F. Sadeghfar, "Synthesis of Fe_3O_4@$_2$P-CNTs magnetic nanocomposite for sonochemical-assisted sorption and pre-concentration of trace Allura Red from aqueous samples prior to HPLC-UV detection: CCD-RSM design," *Ultrasonics Sonochemistry*, vol. 44, pp. 240–250, 2018.

[25] T. Bayram, S. Bucak, and D. Ozturk, "BR13 dye removal using sodium dodecyl sulfate modified montmorillonite: equilibrium, thermodynamic, kinetic and reusability studies," *Chemical Engineering and Processing-Process Intensification*, vol. 158, article 108186, 2020.

[26] S. Banerjee, R. K. Gautam, A. Jaiswal, M. C. Chattopadhyaya, and Y. C. Sharma, "Rapid scavenging of methylene blue dye from a liquid phase by adsorption on alumina nanoparticles," *RSC Advances*, vol. 5, no. 19, pp. 14425–14440, 2015.

[27] G. Sriram, U. T. Uthappa, R. M. Rego et al., "Ceria decorated porous diatom-xerogel as an effective adsorbent for the efficient removal of Eriochrome Black T," *Chemosphere*, vol. 238, article 124692, 2020.

[28] J. W. Lye, N. Saman, S. S. Sharuddin et al., "Removal performance of tetracycline and oxytetracycline from aqueous solution via natural zeolites: an equilibrium and kinetic study," *Clean-Soil, Air, Water*, vol. 45, no. 10, 2017.

[29] A. Younes, S. S. Petros, A. A. Nada et al., "Elaboration of porous alumina nanofibers by electrospinning and molecular layer deposition for organic pollutant removal," *Colloids and Surfaces A: Physicochemical and Engineering Aspects*, vol. 628, article 127274, 2021.

[30] A. Alcantara-Cobos, M. Solache-Rios, and E. Gutiérrez-Segura, "Nobel materials (ZnO nanoparticles and ZnO nanoparticles supported on a zeolite) for the removal of tartrazine from aqueous solutions," *Water, Air, and Soil Pollution*, vol. 230, no. 8, 2019.

[31] D. A. Morales-Serrato, J. Torres-Pérez, Á. de Jesús Ruíz-Baltazar, and S. Y. Reyes-López, "Effect of Zn nanoparticles doping on oxytetracycline removal by natural aluminosilicate and carbon nanotubes," *Water, Air, & Soil Pollution*, vol. 233, no. 2, pp. 1–21, 2022.

[32] C. Gu, K. G. Karthikeyan, S. D. Sibley, and J. A. Pedersen, "Complexation of the antibiotic tetracycline with humic acid," *Chemosphere*, vol. 66, no. 8, pp. 1494–1501, 2007.

[33] X. Liu, H. Zhang, Y. Luo, R. Zhu, H. Wang, and B. Huang, "Sorption of oxytetracycline in particulate organic matter in soils and sediments: roles of pH, ionic strength and temperature," *Science of the Total Environment*, vol. 714, article 136628, 2020.

[34] A. K. Ávila-Martínez, J. H. Roque-Ruiz, J. Torres-Pérez, N. A. Medellín-Castillo, and S. Y. Reyes-López, "Allura Red dye sorption onto electrospun zirconia nanofibers," *Environmental Technology and Innovation*, vol. 18, article 100760, 2020.

[35] S. Herrera-García, M. Aguirre-Ramírez, and J. Torres-Pérez, "Comparison between Allura Red dye discoloration by activated carbon and azo bacteria strain," *Environmental Science and Pollution Research*, vol. 27, no. 23, pp. 29688–29696, 2020.

[36] M. Wawrzkiewicz and Z. Hubicki, "Kinetic studies of dyes sorption from aqueous solutions onto the strongly basic anion-exchanger Lewatit MonoPlus M-600," *Chemical Engineering Journal*, vol. 150, no. 2–3, pp. 509–515, 2009.

[37] M. Wawrzkiewicz and Z. Hubicki, "Kinetics of Adsorption of Sulphonated Azo Dyes on Strong Basic Anion Exchangers," *Environmental Technology*, vol. 30, no. 10, pp. 1059–1071, 2009.

[38] R. Ullah, F. J. Iftikhar, M. Ajmal et al., "Modified clays as an efficient adsorbent for brilliant green, ethyl violet and allura red dyes: kinetic and thermodynamic studies," *Polish Journal of Environmental Studies*, vol. 29, no. 5, pp. 3831–3839, 2020.

[39] F. O. Erdoğan, "Comparison of activated carbon produced from carob stones with 4a zeolite for allura red AC dye," *Journal of Science and Technology*, vol. 9, no. 1, pp. 75–79, 2019.